DC Injection Suppression in a Transformer-Less T-Type Grid-Connected Converter Using an Improved SWDIM and Fuzzy-Fractional PID Controller

Jingmei Guo, Chao Sheng, Pandian Luo, Jian Zhang, Zhengjun Shi

Abstract-**Owing to the scaling and zero-drift phenomena exhibited by current sensors during sampling, tolerances, and the time-delay associated with gate-driving power transistors in practical applications, direct current (DC) offsets commonly manifest within the grid current. This phenomenon has the potential to degrade the power quality of the grid current. Consequently, numerous techniques, such as the employment of physical blocking capacitors and virtual capacitors, have been developed to maintain the DC current within the IEEE 1547-2018 standards. However, these methodologies are associated with drawbacks such as prolonged response times, intricate control algorithms, additional power dissipation (e.g., physical blocking capacitors), and increased costs. To address these challenges, an enhanced DC current detection method is introduced, which utilizes a prediction model and sliding-window-double-integration (SWDIM) technique to extract the DC component from the predicted grid current. The implementation of a Fuzzy fractional-order Proportional-Integral-Derivative (FOPID) controller, based on the Caputo derivative, facilitates the effective suppression of the DC current, offering superior steady-state and dynamic response compared to existing approaches. A hardware setup comprising a three-level T-type (3LT^{2}C) grid-connected converter has been constructed. Simulation and experimental results demonstrate that the proposed scheme exhibits enhanced DC current suppression performance compared to existing methodologies under various scenarios.**

Keywords- **Transformer-less, dc current, virtual capacitor, time-delay, model-predictive-control (MPC), power quality.**

I. Introduction

In recent years, more and more renewable energy such as PV (Photovoltaic) and wind power are integrated to the distributed power network, typically, voltage and current source power converters are usually served as the grid-connected interface. Conventional grid-connected converter system (GCCs), e.g., three-phase grid-connected converter, has a fundamental frequency isolation transformer that is used for voltage matching and electrical isolation, where the dc-link voltage does not need to be high enough to satisfy the grid integration requirements. However, the isolation transformer based GCCs has the disadvantages of large volume, noise, weight, and low efficiency [1, 2].

To solve these problems, non-isolated GCCs has been more popular nowadays, which has the merits of low cost, no noise, small volume, and high efficiency [3]. For non-isolation GCCs, the dc injection becomes a big problem. It has been reported that dc injection can cause the saturation of the transformer, accelerate the corrosion of the network cabling, endanger the safe operation of the power devices, generate obvious torque ripple and overheat of the ac motor, etc. [4, 5]. To avoid dc current injection, several international standards were established by some countries and organizations [6]. In [7] and , it was required that the dc current being injected into the grid must be less than 0.5% of the rated current. In Japan, dc current in the grid current must be less than 20 mA .

There are many reasons that may lead to dc current injection [8, 9]. Typically, asymmetry of the switching behavior of the power transistors, the possible mismatch in the alignment of the gate drive signals, the zero-drift in the current and voltage measurement may also generate dc current in the grid current. In grid current control, the reference current generated by analogy circuit may also contain unexpected dc current. To prevent from dc current injection, many research works have been put forward [10-12]. And the dc suppression methods are categorized by three types.

(1) Power converter with dc current suppression capability. The grid-connected converter itself has the capability of preventing dc current injection, such as half-bridge converter [13] or three-level diode clamped converter [8], etc. In these converters, usually a capacitor is inserted in the current path. Hence, the dc current is physically blocked. However, a higher dc-link voltage is required for half-bridge converter to satisfy grid connected condition, resulting higher voltage stress and power losses for the power transistors.

(2) Detection and compensation method [12, 14]. In [15], to measure milliamperes dc current mixed in large (≥10 A peak) ac current, a novel current sensor (CS) was proposed, which used a current transformer (CT), a power amplifier, and an additional winding to cancel the ac magnetic field in a commercial current sensor (CCS). Under this circumstance, the CCS is used to detect the remaining small dc magnetic

Manuscript received Nov 28, 2024; revised Feb 13, 2025.

This work was supported by Guangdong Provincial Key Laboratory of New Technology for Smart Grid, China Southern Power Grid Technology Co., Ltd Guangzhou, Guangdong 5100, China. NO: 2021YFB38002000.

Jinmei Guo is a senior engineer at Guangdong Provincial Key Laboratory of New Technology for Smart Grid, China Southern Power Grid Technology Co., Ltd. Guangzhou, Guangdong 5100, China (email: gjm_gddky@163.com).

Chao Sheng is a professor level senior engineer at Guangdong Provincial Key Laboratory of New Technology for Smart Grid, China Southern Power Grid Technology Co., Ltd. Guangzhou, Guangdong, China,5100, China (email: chaosheng@gd.csg.cn).

Pandian Luo is an engineer at Guangdong Provincial Key Laboratory of New Technology for Smart Grid, China Southern Power Grid Technology Co., Ltd. Guangzhou, Guangdong 5100, China (Email: Pdluo @163.com).

Jian Zhang is an engineer at Guangdong Provincial Key Laboratory of New Technology for Smart Grid, China Southern Power Grid Technology Co., Ltd. Guangzhou, Guangdong 5100, China (email: zhangjian@gd.csg.cn).

Zhengjun Shi is an engineer at Guangdong Provincial Key Laboratory of New Technology for Smart Grid, China Southern Power Grid Technology Co., Ltd. Guangzhou, Guangdong 5100, China (email: zjshi@gd.csg.cn).

fields. As the range of CCS does not need to be large, the dc current measurement error was significantly reduced. Typically, the auto-calibration dc-link current sensing technique, in which a parallel transformer is utilized for current detection. In [16], a two-stage resistive-capacitor (RC) circuit detection method for dc current detection was proposed. In [12], a magnetic saturation detection method using hall sensor was used. In [12], a new technique was proposed to measure dc current component with high accuracy using a coupled inductor combined with a small-range Hall effect current sensor for achieve the lowest possible cost with the highest possible accuracy. In [17], an active dc suppression method was proposed, in which the dc current injection was accurately determined by extracting the line-frequency component from inverter dc-link current measurements, and then, mitigated with an active closed-loop controller. The latest research work on dc current compensation with intelligent control has been found to have good performance. However, it needs high-speed microprocessor for massive data storing and float-point calculation [18]. Usually, compared with the rated grid current, the dc current is quite small, the performance of the current detection and compensation method is quite relied on the sampling accuracy of the current sensor. In [19], sliding-window-integration-method (SWIM) was proposed for fast dc current extraction, and then compensation was carried out by an adaptive Back-Propagation (BP) - Proportional-Integral-Derivative (PID) (BP-PID) controller based on neural network (NN). In [20, 21], Fractional-order proportional-integral-derivative (FOPID) controllers have been employed in the power converter systems and demonstrated better performance than their integer-order counterparts.

(3) Physical and virtual capacitor methods [18, 22]. The idea is based on the dc mitigation of capacitors. In physical capacitor dc suppression method, the blocking capacitors are inserted into the grid current path of the circuit. However, this method has the many disadvantages [23], i.e., malfunction of the capacitors may disconnect the converter from the grid, which may leads to breakdown of the whole system. To prevent the capacitors from disconnecting with the grid, an auxiliary circuit are needed, which increase the control complexity of the circuit. Moreover, to realize the loop-gain across the capacitor at the fundamental frequency to be approximately close to 1, a relatively large capacitance should be selected. However, this will increase the cost and volume of the GCCs. To solve this problem, the concept of virtual capacitors was presented, which utilizes a closed-loop control to achieve equivalent performance of a real capacitor for dc current blocking [22, 24]. Compared to physical capacitors, this approach eliminates the necessity for an additional DC current detection circuit. DC suppression performance can be attained by modifying the virtual capacitor within the software, offering greater flexibility albeit at a higher cost. Nonetheless, the selection of the virtual capacitance must be adjusted according to the DC current content, which involves complex calculations.

Based on the literature review, this paper endeavors to identify a direct current (DC) suppression method characterized by simplicity in control, rapid response, and high precision. A novel DC current detection and suppression approach, founded on an enhanced Switched-Winding Dual Inductor Module (SWDIM) technique coupled with a Fuzzy-Fractional-Order Proportional-Integral-Derivative (Fuzzy-FOPID) controller, is presented for the mitigation of DC injection. In summary, the principal contributions of this paper can be delineated as follows:

1)A novel Sliding-Window-Double-Integration Method (SWDIM) predicated on the predicted grid current, referred to as SWDIM-P, is presented. This approach mitigates time-delay through multi-step prediction and yields results closer to the actual values compared to conventional methodologies. Consequently, SWDIM-P offers superior accuracy over existing SWDIM detection schemes.

2)To address the time-delay inherent in Model Predictive Control (MPC) implementation, a two-step prediction methodology is proposed.

3)A Fuzzy-Fractional-Order Proportional-Integral-Derivative (Fuzzy-FOPID) current controller is introduced to achieve rapid and high-precision DC current suppression, along with other control objectives. This controller demonstrates faster and improved performance relative to existing methods.

This paper is organized as follows. In Section II, the topology and prediction model of $3LT^2C$ LCL-GCC are introduced. In Section III, the proposed dc current detection and suppression method are introduced. In Section IV, comparisons of various dc current suppression methods are carried out by simulation verification. In Section V, experimental results are provided to validate the effectiveness of the proposed method. Finally, Section VI concludes this paper.

II. Model Predictive Control Of The LCL-GCC Converter

A. Topological Description

Fig.1 shows the topology of a $3LT^2C$ system. The DC-bus side consists of two series-connected capacitors C_1 and C_2, whose voltages are u_p and u_n, respectively. $3LT^2C$ is connected with an LCL filter. Its parameters include the converter-side inductance L_1, grid-side inductance L_2, and filter capacitor C_f. R_1 and R_2 are the parasitic resistances of L_1 and L_2, respectively. i_{np} is the neutral-point (NP) current. v_i, i_1 , i_2, v_C, i_g, and v_g are the converter-side voltage (the voltage from the converter output point to the neutral point O), converter-side current, grid-side current, filter-capacitor voltage, point of common coupling (PCC) current, and grid voltage, respectively.

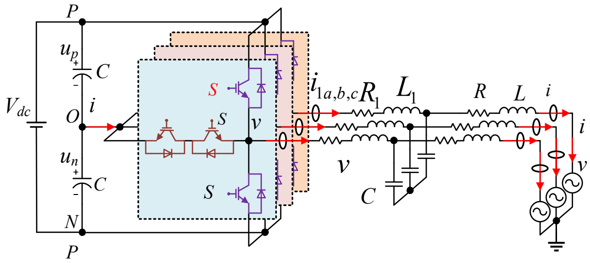

Fig. 1. Topology of a $3LT^2C$ system.

B. Prediction Model of the $3LT^2C$

In each phase of a $3LT^2C$, there are three switching states: [P], [O], and [N]. The corresponding relationships between these three switching states and the four switching devices in each phase are summarized in Table I. Thus, $3LT^2C$ has a total of 27 switching state combinations, which can be interpreted as CVVs for the FCS-MPC.

TABLE I
OUTPUT OF THE T-TYPE CONVERTER

Switching state	S_{i1}	S_{i2}	S_{i3}	S_{i4}
[P]	on	on	off	off
[O]	off	on	on	off
[N]	off	off	on	on

At any given instance, the CVV can be defined as

$$\begin{aligned} &\boldsymbol{u}^{(x)} = [u_a, u_b, u_c]^T \\ &\text{s.t. } u_a, u_b, u_c \in \{-1, 0, 1\} \ x = 1, 2 \end{aligned} \quad , \tag{1}$$

where -1, 0, and 1 represent the [N], [O], and [P] states, respectively. (x) represents the number of converters, and the formula not marked with (x) is used for both converters unless otherwise specified.

Assuming a balanced NP voltage, the converter-side voltage can be written as

$$\boldsymbol{v}_i = \frac{V_{dc}}{2}\boldsymbol{u} \quad , \tag{2}$$

where $\boldsymbol{v}_i = [v_{ia}, v_{ib}, v_{ic}]^T$.

According to Kirchhoff's law, and assuming that the three-phase circuit is symmetrical, the circuit equation for the LCL filter can be derived as follows:

$$\begin{cases} \dfrac{d\boldsymbol{i}_1}{dt} = -\dfrac{R_1}{L_1}\boldsymbol{i}_1 - \dfrac{1}{L_1}\boldsymbol{v}_C + \dfrac{V_{dc}}{2L_1}\boldsymbol{u} \\ \dfrac{d\boldsymbol{i}_2}{dt} = -\dfrac{R_2}{L_2}\boldsymbol{i}_2 + \dfrac{1}{L_2}\boldsymbol{v}_C - \dfrac{1}{L_2}\boldsymbol{v}_g \\ \dfrac{d\boldsymbol{v}_C}{dt} = \dfrac{1}{C_f}\boldsymbol{i}_1 - \dfrac{1}{C_f}\boldsymbol{i}_2 \end{cases} , \tag{3}$$

where $\boldsymbol{i}_1 = [i_{1a}, i_{1b}, i_{1c}]^T$, and the remaining bold vectors are expressed similar to $\boldsymbol{i}_1$.

After Clark transformation, the state model is rewritten as follows:

$$\frac{d\boldsymbol{x}(t)}{dt} = \boldsymbol{F}\boldsymbol{x}(t) + \boldsymbol{G}\boldsymbol{u}(t) + \boldsymbol{P}\boldsymbol{v}_g(t) \quad , \tag{4}$$

where $\boldsymbol{x}(t) = [i_{1\alpha}(t), i_{1\beta}(t), i_{2\alpha}(t), i_{2\beta}(t), v_{C\alpha}(t), v_{C\beta}(t)]^T$,

$$\boldsymbol{F} = \begin{bmatrix} -\dfrac{R_1}{L_1}\boldsymbol{I}_{2\times2} & \boldsymbol{O}_{2\times2} & -\dfrac{1}{L_1}\boldsymbol{I}_{2\times2} \\ \boldsymbol{O}_{2\times2} & -\dfrac{R_2}{L_2}\boldsymbol{I}_{2\times2} & \dfrac{1}{L_2}\boldsymbol{I}_{2\times2} \\ \dfrac{1}{C_f}\boldsymbol{I}_{2\times2} & -\dfrac{1}{C_f}\boldsymbol{I}_{2\times2} & \boldsymbol{O}_{2\times2} \end{bmatrix}, \boldsymbol{G} = \begin{bmatrix} \dfrac{V_{dc}}{2L_1}\boldsymbol{I}_{2\times2} \\ \boldsymbol{O}_{4\times2} \end{bmatrix}\boldsymbol{C}_{3s/2s},$$

$$\boldsymbol{P} = \begin{bmatrix} \boldsymbol{O}_{2\times2} \\ -\dfrac{1}{L_2}\boldsymbol{I}_{2\times2} \\ \boldsymbol{O}_{2\times2} \end{bmatrix}\boldsymbol{C}_{3s/2s}, \boldsymbol{C}_{3s/2s} = \frac{2}{3}\begin{bmatrix} 1 & -\dfrac{1}{2} & -\dfrac{1}{2} \\ 0 & \dfrac{\sqrt{3}}{2} & -\dfrac{\sqrt{3}}{2} \end{bmatrix}.$$

By using the Du Hamel formula [25] to discretize (4), the discretized-time state equation can be obtained as follows:

$$\boldsymbol{x}(k+1) = \boldsymbol{A}\boldsymbol{x}(k) + \boldsymbol{B}\boldsymbol{u}(k) + \boldsymbol{T}\boldsymbol{v}_g(k) \quad , \tag{5}$$

where $\boldsymbol{A} = e^{\boldsymbol{F}T_s}, \boldsymbol{B} = -\boldsymbol{F}^{-1}(\boldsymbol{I} - \boldsymbol{A})\boldsymbol{G}, \boldsymbol{T} = -\boldsymbol{F}^{-1}(\boldsymbol{I} - \boldsymbol{A})\boldsymbol{P}$, and T_s represent the sampling interval.

NP voltage fluctuation is an inherent problem in a three-level topology. The two series-connected DC-bus capacitors should evenly divide the DC-bus voltage to ensure a voltage accuracy of (2). Let $C_1 = C_2$, and the NP voltage is defined as follows:

$$u_{np} = u_n - u_p \quad . \tag{6}$$

Then, according to Kirchhoff's current law, the NP current can be rewritten as follows:

$$i_{np} = -(|u_a| i_{1a} + |u_b| i_{1b} + |u_c| i_{1c}) = -C_1 \frac{du_{np}}{dt} \quad . \tag{7}$$

By forward Euler discretization, the NP voltage in one switching period can be expressed as follows:

$$u_{np}(k+1) = \frac{T_s}{C_1}|\boldsymbol{u}(k)|^T \boldsymbol{i}_1(k) + u_{np}(k) \quad . \tag{8}$$

C. Time-Delay Elimination by Two-Step Prediction

At instant k, the reference tracking and optimal switching sequence are evaluated by the N-step cost function, that is, the future finite number of predicted switching sequences are included in $\boldsymbol{v}(k)$ and compiled to minimize the cost function. When the state equation is continuously applied to multi-step prediction, we have

$$\begin{aligned} \boldsymbol{x}(k+1) &= \boldsymbol{A}\boldsymbol{x}(k) + \boldsymbol{B}\boldsymbol{v}(k) + \boldsymbol{T}\boldsymbol{v}_g(k) \\ \boldsymbol{x}(k+2) &= \boldsymbol{A}\boldsymbol{x}(k+1) + \boldsymbol{B}\boldsymbol{v}(k+1) + \boldsymbol{T}\boldsymbol{v}_g(k+1) \\ &= \boldsymbol{A}^2\boldsymbol{x}(k) + \boldsymbol{A}\boldsymbol{B}\boldsymbol{v}(k) + \boldsymbol{A}\boldsymbol{T}\boldsymbol{v}_g(k) + \boldsymbol{B}\boldsymbol{u}(k+1) \\ &\quad + \boldsymbol{T}\boldsymbol{v}_g(k+1) \\ \boldsymbol{x}(k+3) &= \boldsymbol{A}^3\boldsymbol{x}(k) + \boldsymbol{A}^2\boldsymbol{B}\boldsymbol{v}(k) + \boldsymbol{A}\boldsymbol{B}\boldsymbol{v}(k+1) + \boldsymbol{B}\boldsymbol{v}(k+2) \\ &\quad + \boldsymbol{A}^2\boldsymbol{T}\boldsymbol{v}_g(k) + \boldsymbol{A}\boldsymbol{T}\boldsymbol{v}_g(k+1) + \boldsymbol{T}\boldsymbol{v}_g(k+2) \\ &\quad + \boldsymbol{A}^2\boldsymbol{T}\boldsymbol{v}_g(k) + \boldsymbol{A}\boldsymbol{T}\boldsymbol{v}_g(k+1) + \boldsymbol{T}\boldsymbol{v}_g(k+2) \\ \boldsymbol{x}(k+\mathrm{N}) &= \boldsymbol{A}^N\boldsymbol{x}(k) + \boldsymbol{A}^{N-1}\boldsymbol{B}\boldsymbol{v}(k) + \cdots + \boldsymbol{A}^0\boldsymbol{v}(k+N-1) + \\ &\quad \boldsymbol{A}^{N-1}\boldsymbol{T}\boldsymbol{v}_g(k) + \boldsymbol{A}^{N-2}\boldsymbol{T}\boldsymbol{v}_g(k+1) + \cdots + \boldsymbol{A}^0\boldsymbol{v}_g(k+N-1) \\ \boldsymbol{x}(k+\mathrm{m}) &= \boldsymbol{A}^m\boldsymbol{x}(k) + \sum_{l=0}^{m-1}\boldsymbol{A}^{m-1-l}\boldsymbol{B}\boldsymbol{v}(k+l) + \sum_{l=0}^{m-1}\boldsymbol{A}^{m-1-l}\boldsymbol{T}\boldsymbol{v}_g(k+l) \end{aligned}$$

where m=1, ..., N. The rows of each zero matrix are the same as that of $\boldsymbol{C}$ matrix, and the number of columns is the same as that of $\boldsymbol{B}$ matrix. In digital implementation, it is impossible to achieve current sampling, control algorithm implementation as well as changing rectifier switch state in one sampling cycle. There has some delay in dealing with vector selection. To solve this problem, a two-step predictive model predictive current control algorithm is adopted here, the optimal output vector of k+2 is calculated at k and output at k+2, which avoids the time-delay in existing dc current suppression schemes.

Fig.2 (a) shows the calculation-delay diagram of one-step predictive. The system samples current and voltage values at instant k. In ideal state, the algorithm runs in an instant, then the system will calculate the optimal candidate vector and change the switching state of the rectifier bridge at k. In practice, due to the implementation time, the conversion of the rectifier switching state must last some time. Therefore, the switch state that should be output at instant k will last some delay after T_S^*. it will output at k'. Since the switching state of LCL-GCC does not change during T_S^*, the optimal vector calculated in the previous period is still used. As a result, the selected optimal vector cannot be implemented completely in one sampling period T_s.

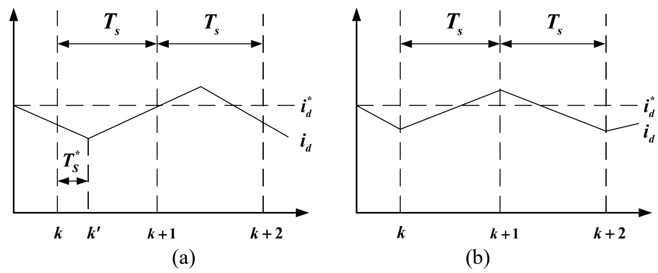

Fig. 2. Calculation delay in predictive control. (a). One-step prediction; (b). Two-step prediction.

Fig.2 (b) is the schematic diagram of a two-step prediction method. The method predicts various state variables at k+1, and then predicts state variables at $k+2$. Since the switching state of the system at $k \sim k+1$ has been determined by previous control period, it is not a controllable quantity. Therefore, in cost function design of MPC controller, the absolute value of the difference between the predicted current at $k+2$ and the current reference at $k+2$ should be taken as the benchmark to obtain the optimal vector, and the optimal vector are selected at instant $k+1$, thus avoiding the time-delay.

D. Design of Cost Function (CF)

The design of the CF for 3LT^{2}C involves grid-current tracking and NP voltage control, which are explained as follows:

CF for grid-current tracking: The control objective is to track the state variables of the LCL-GCC with active damping (namely, grid-side current, converter-side current, and capacitor voltage), then the cost function for MPC controller is written as

$$J_x = \lambda_1 \left| i_{1\alpha\beta} - i_{1\alpha\beta}^* \right| + \lambda_2 \left| i_{g\alpha\beta} - i_{g\alpha\beta}^* \right| + \lambda_3 \left| v_{c\alpha\beta} - v_{c\alpha\beta}^* \right| \quad (9)$$

Where λ_1, λ_2 and λ_3 are the coefficients of the cost function. When a minimum J is selected, the candidate vector $\boldsymbol{v}(k)$ is the optimal switching vector. Through the sampling circuit, each state variable is input to MPC controller, and the above operation is repeated to form a closed-loop control, achieving multi-objective control of the system.

CF for NP voltage control: The second CF is the balance of the NP voltage. The predictive NP voltage relationship derived from (8) can be directly used in the CF as follows:

$$J_{np} = \left| u_{np}(k+1) - 0 \right| = \left| \frac{T_s}{C_1} \left| \boldsymbol{u}(k) \right|^T \boldsymbol{i}_1(k) + u_{np}(k) \right| \quad .(10)$$

Thus, the overall cost function of the system is given by

$$J = J_x + J_{np} \quad (11)$$

III. DC Current Suppression Based On Fuzzy-PI-MPC Controller

A. DC current Detection Based on SWDIM-P Method

For various dc current suppression methods, accurate extraction of dc current plays an importance role. According to IEEE standard-1325, dc current should be limited within 0.5% of the rated current. The hall sensor used to sample current in traditional GCC features with small size, wide bandwidth range and isolated output, which makes it widely used in industry. Considering the fast response and accuracy of dc current detection, a dc current detection method based on sliding window integral of the predicted grid current is introduced. The integral detection method proposed in [26, 27] is to eliminate the fundamental and harmonic components of the grid current by multiple integration, and only the dc current is retained. From (5), the discrete prediction model of the grid current is given as (12). In general, considering the dc and ac contents of the grid current, the overall expression of i_{gp} can be obtained as (13)

$$\boldsymbol{i}_{gp}(k+1) = \boldsymbol{A}\boldsymbol{i}_g(k) + \boldsymbol{B}\boldsymbol{v}(k) + \boldsymbol{T}\boldsymbol{v}_g(k) \quad (12)$$

$$\begin{aligned} i_{gp}(t) &= i_{dcp} + i_{ac} \\ &= i_{dcp} + \sum\nolimits_{n=1,2,3,L} I_n \sin(2\pi n f_1 + \varphi_n) \end{aligned} \quad (13)$$

where i_{ac} is the ac component of the predicted grid current, i_n, nf_1 and φ_n are the amplitude, frequency and phase of ac component respectively, i_{dcp} is the predicted dc current in grid current. In an ideal situation, when the ac component in the predicted grid current is a sine wave, the average current value in a period T is 0. Therefore, (14) is obtained by integrating (13)

$$\frac{1}{T}\int_{t_0}^{t_0+T} i_{gp}(t)dt = \frac{1}{T}\int_{t_0}^{t_0+T} i_{dcp}(t)dt + \frac{1}{T}\int_{t_0}^{t_0+T} i_{ac}(t)dt = i_{dcp} \quad (14)$$

$$i_{dcp}(k) = \frac{1}{N}\sum\nolimits_{K=0}^{N-1} i_{gp}(k) \quad (15)$$

Thus, the predicted dc current i_{dcp} is obtained. Assuming that N samples are collected within a given period of grid current, the discrete expression of the k-th predicted grid current $i_{gp}(k)$ is obtained, to achieve (16) without additional computational burden, the sliding window iterative algorithm is used [28]. Then the periodic integral can be updated with the arrival of each new sample. In this way, a rolling average of the last 360° of the fundamental frequency is obtained, which effectively generates a real-time update of the dc current, as shown in Fig.5. This can be expressed as

$$i_{dcp}(k) = \frac{1}{N}\sum\nolimits_{K=N_{now}-N+1}^{N_{now}} i_{gp}(k) \quad (16)$$

In (16), Initially, the calculation starts from $i_{gp}(N_{now} - (N-1))$ to $i_{gp}(N_{now})$ are the average value of the first N samples. In the next discrete step, the average value changes from $i_{gp}(N_{now} - (N-2))$ to $i_{gp}(N_{now}+1)$. If the system is running, the iterative process will continue. Since the average calculation is repeated at each sampling point, the influence of noise is greatly suppressed, and the robustness of dc voltage offset detection is guaranteed. Attenuation output fundamental frequency and grid frequency f_0 is the same.

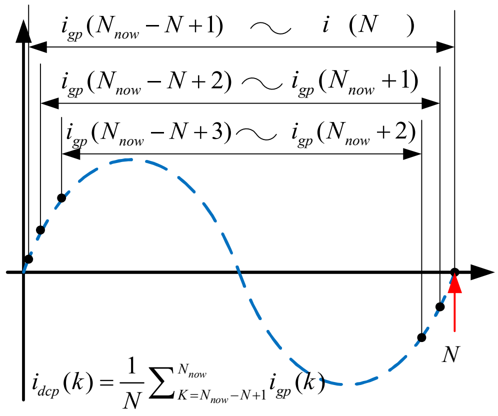

Fig. 3. Integral diagram of sliding window method.

B. Error Analysis of dc Current Detection

In fact, the grid current is non-sinusoidal, so the integral of ac component in (16) is not equal to 0, the ac component integral is rewritten by

$$\begin{aligned} e &= \frac{1}{T}\int_{t_0}^{t_0+T} i_{ac}(t)\,dt \\ &= \frac{1}{T}\sum_{n=1,2,3,L} \frac{i_n}{\pi n f_1} \sin\begin{pmatrix} 2\pi n f_1 t \\ +\varphi_n + \pi n f_1 T \end{pmatrix} \sin(\pi n f_1 T) \end{aligned} \tag{17}$$

Because $T = 1/f_0$ and $f_0 \neq f_1, f_0$ is the grid frequency, substituting into (17) yields

$$e = \sum_{n=1,2,3,L} \frac{f_0 i_n}{\pi n f_1} \sin(\pi n f_1 / f_0) \sin\begin{pmatrix} 2\pi n f_1 t + \varphi_n + \\ \pi n f_1 / f_0 \end{pmatrix} \tag{18}$$

Therefore, the predicted dc current is rewritten as

$$i_{dcp} = \frac{1}{T}\int_{t_0}^{t_0+T} i_{gp}(t) = i_{dcp} + e \tag{19}$$

It can be seen from the above results that the error of dc current prediction value is e and the error amplitude is $f_0 i_n/(\pi n f_1)\sin(\pi n f_1/f_0)$. As time goes on, the denominator approaches infinity and the error e approaches 0. On the one hand, the predicted dc current is based on the iterative algorithm using sliding window. According to the principle of the algorithm, the integral of ideal ac component is not equal to 0 in the iteration process of less than one cycle. Therefore, it needs at least one fundamental frequency cycle sampling value to accurately predict the dc current. However, the predicted dc current can be accurately obtained after 0.02 s, which shows the rapidity of the proposed method.

On the other hand, traditional dc current detection is based on the sensor acquisition, which cannot avoid the scaling error and sampling time error, resulting in inaccurate results. The proposed dc current detection method (SWDIM-P) is based on the predicted grid current from the prediction model. It can eliminate the time-delay through multi-step prediction, which is closer to the actual value than traditional method. Therefore, SWDIM-P is more accurate than existing SWDIM as well as sliding-window-single-integration-method (SWSIM) detection scheme, which will be verified by the simulation and experiment results.

C. Design of Fuzzy-FOPID Controller for DC Injection Suppression

To have better dc injection performance of the 3LT^{2}C system, the fractional-order PI controller is presented. The proportion controller will make the system state approach to the goal rapidly. The integral controller will make the trajectory better closing to the goal [21, 29]. Thus, the expression of a FOPIC controller is given as:

$$u_i = -K_p x_i - K_i D_t^q x_i \tag{20}$$

Where K_p is the proportion coefficient, K_i is the integral coefficient. The controller parameters K_p and K_i will affects the output of the controller directly. D_t^q is the Caputo fractional derivative of the FOPID controller.

D. Overall DC Injection Suppression Scheme

In order to effectively suppress the direct current (DC), a novel control strategy that eliminates the need for an isolation transformer and is founded on a predictive model is presented. The complete block diagram is illustrated in Fig. 4. The operational implementation of the proposed DC injection suppression approach is detailed as follows:

Firstly, various state variables are sampled, and their values are inputted into the model. The predicted grid current at k+1 is determined by the predictive model. This predicted grid current is detected using the enhanced sliding window double integration method to extract the DC component, which is subsequently inputted into the current controller. To achieve a more rapid suppression of the DC current, a Fuzzy-Fractional Order Proportional-Integral-Derivative (Fuzzy-FOPID) controller is employed. The negative feedback is then fed back to the reference, and ultimately inputted into the cost function to derive the optimal switching sequence. Owing to the high robustness and swift response characteristics of the predictive model, the DC current can be rapidly and accurately suppressed.

In addition, Fuzzy-FOPID controller retains the last K_p, K_i values K_P^*, K_i^*, and then adds the fuzzy controller values ΔK_p, ΔK_i, and then acts on the control object. The initial values K_p^* and K_i^* are set according to experience, Namely

$$K_p = K_P^* + \Delta K_p \tag{21}$$

$$K_i = K_i^* + \Delta K_i \tag{22}$$

To improve the effect of dc current suppression, the detection of dc current tracking error E and its deviation change rate E_c are selected as the inputs of the Fuzzy controller, $\Delta K_p, \Delta K_i$ is the output variable of fuzzy controller. The four fuzzy sets are defined as {NB, MN, NS, O, PS, PM, PB}, and the universe of the four variables is defined as {- 6, - 5, - 4, - 3, - 2, - 1, 0, 1, 2, 3, 4, 5, 6}, The membership functions of the input variable deviation E and deviation change value E_c and the membership functions of the output variables ΔK_p and ΔK_i are shown in Fig. 5.

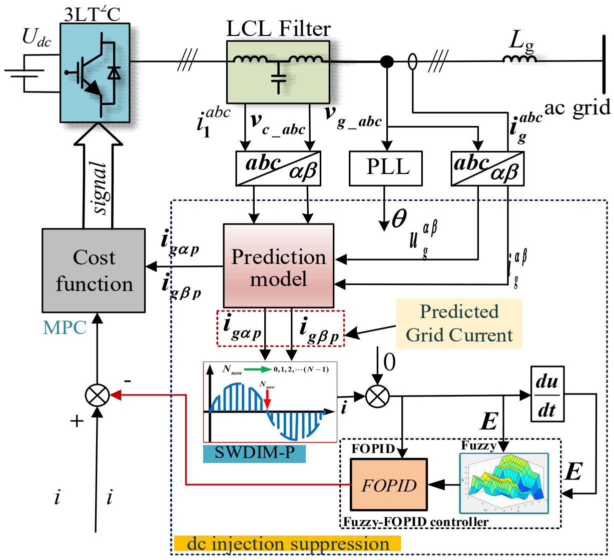

Fig. 4. SWDIM-P based dc current suppression with a Fuzzy-FOPID controller.

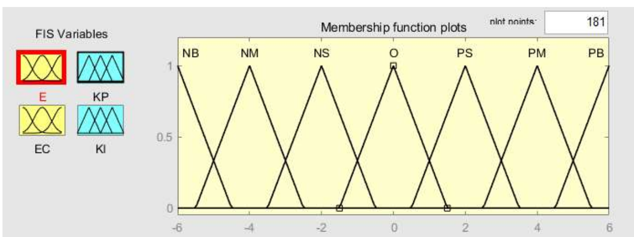

Fig. 5. Membership functions of the input variables E and E_c, output variables ΔK_p, ΔK_i in Fuzzy controller.

IV. Simulation Analysis

A. Parameter Specification

To prove the effectiveness of the proposed method, the Simulation model is built in MATLAB/Simulink, and the system parameters are given in Table I.

TABLE II
PARAMETER SPECIFICATIONS FOR SIMULATION

Symbol	Parameter	Values
P_e	Rated power	10 kW
V_{dc}	DC-link voltage	500 Vdc
e_g	Grid voltage (RMS)	220 Vac
f_g	Fundamental frequency of the grid	50 Hz
C_{dc}	DC-link capacitance	3 mF
L_1	Converter-side inductance	2 mH
L_2	Grid-side inductance	1 mH
L_g	Grid inductance	2 mH
C_f	Filter capacitance.	2.2 μF
f_s	Switching frequency.	25 kHz

TABLE III
SIMULATION PARAMETER SPECIFICATIONS FOR FUZZY-FOPID CONTROLLER

Symbol	Parameter	Values
C_b	Virtual capacitor	50 µF
k_p	Proportional coefficient	500 Vdc
k_i	Integral coefficient	220 Vac
q	Fractional-order	0.8
$\lambda_1, \lambda_2, \lambda_3$	Coefficients for the MPC controller	1, 0.4, 0.2
$i^*_{g\alpha\beta}$	Grid current reference	10 A

B. Result and Analysis

Case I: Comparison of Different DC Current Detection Methods.

Considering the frequency fluctuations, the identical power parameters presented in Table I are utilized. A comparative analysis is conducted between the SWDIM-P method and two other approaches, namely the sliding-window-single-integration-method (SWSIM) and the SWDIM method. The corresponding results are illustrated in Fig. 6. At 0.2 s, when a direct current (dc) of 5 A is detected in the α-phase, the response time of the SWDIM-P scheme and the commonly adopted integration method SWSIM are approximately within one cycle. This observation further corroborates the error analysis delineated in Section III. Conversely, the SWDIM method requires around two cycles for dc current detection. Regarding detection accuracy, Fig. 6 demonstrates that the proposed SWDIM-P method exhibits no significant oscillations, yielding a more precise detection result compared to the other two schemes.

Case II: Comparison of different dc current suppression methods

Under comparable scenarios, the efficacy of the Fuzzy-FOPID controller is substantiated by comparing it with the virtual capacitance and the BP-PID schemes. The comparative results are illustrated in Fig. 7. At 0.2 seconds, a direct current of 5A is induced in the α-phase of the grid current. The virtual capacitance method suppresses this direct current to 0.5% of the rated current (as per IEEE standard Std 1547-2018) in 0.086 seconds, by 0.286 seconds. Conversely, the standard suppression method based on BP-PID requires 0.133 seconds to achieve the same level of suppression. However, by the proposed scheme, the direct current is suppressed to less than 0.5% of the rated current by t=0.238 seconds (with a requirement of 0.038 seconds), marking a 55.8% improvement over the virtual capacitor scheme and a 71.4% enhancement compared to the BP-PID method.

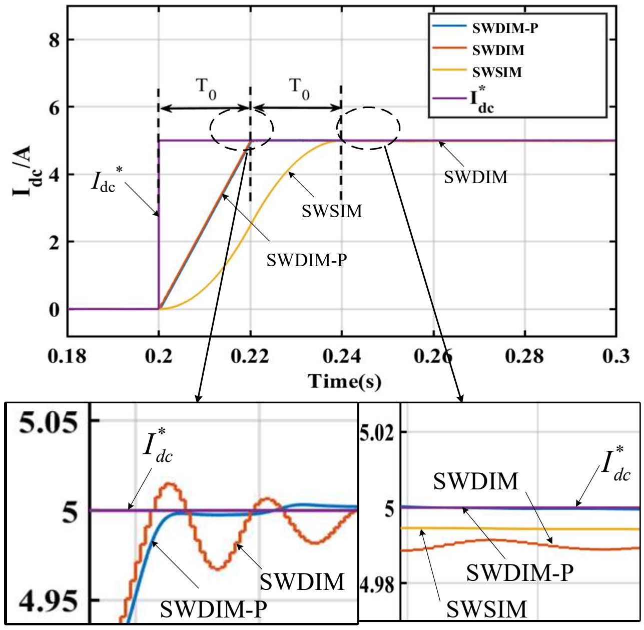

Fig. 6. Comparison of different dc current detection methods.

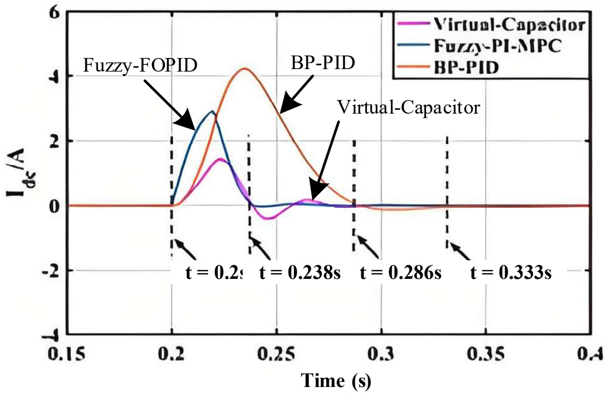

Fig. 7. Comparison of different dc current suppression schemes.

V. Experiment Results

A. Hardware Setup

To further validate the simulation results, a 10-kVA GCCs laboratory prototype has been established (refer to Fig. 8). The hardware prototype employs six N-Channel Power MOSFETs (IRFP460C, 500V/20A, $R_{DS} = 0.24\Omega, V_{GS} = 10$V). The proposed SWDIM-P dc current extraction scheme and Fuzzy-FOPID controller have been implemented using a 32-bit floating-point TMS320F28335 microcontroller, which features a main frequency of 150 MHz and is optimized for processing, sensing, and actuation to improve system performance in real-time control applications. Gate drivers, specifically the 1ED20I12FA2A from Infineon Technologies, have been utilized for MOSFET driving control. ACPL-C790 isolation amplifiers with ±3% gain tolerance and a 200 kHz bandwidth have been designed for current and voltage sensing. The virtual capacitance is chosen as 50 μF. The experimental parameters are identical to the simulation parameters.

It is important to note that, in order to achieve a flexible grid test scenario, a grid emulator, specifically the Chroma 61860, is utilized. The Chroma 61860 is a high-power grid simulation power supply primarily employed for testing photovoltaic inverters, smart grids, and electric vehicle-related products. This device possesses multiple functions and features, enabling it to meet a wide array of testing requirements. The Chroma 61860 is suitable not only for product development stages but also for product quality verification and production stages. Additionally, the device can perform high-voltage-ride-through-testing (HVRT), harmonic analysis, waveform distortion assessment, three-phase imbalance evaluation, voltage sag testing, dc component emulation, short-term interruption testing, and voltage change immunity testing.

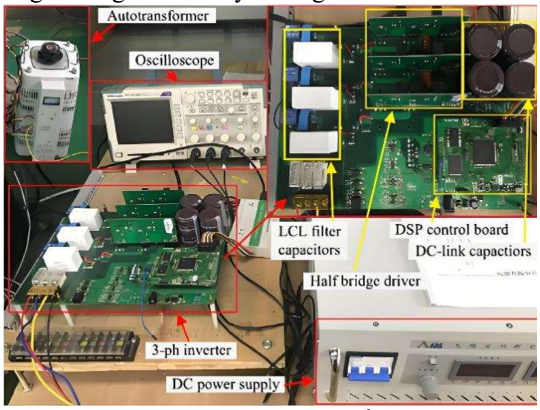

Fig. 8. Experimental setup and designed 3LT^{2}C LCL-type GCCs.

The criteria for evaluating various direct current (DC) current detection and suppression methods are presented as follows: 1) In terms of DC current detection, a method that yields a more accurate detection result with a rapid response is considered superior. 2) Regarding DC current suppression, the control method capable of achieving fast DC current suppression performance would be regarded as the optimal technique.

B. Experimental Results and Analysis

To ascertain the efficacy of the proposed methodology, the subsequent five test scenarios are evaluated:

Case I: Utilizing solely the traditional MPC controller, with no dc current suppression method employed. The waveform of the three-phase grid current is presented in Fig.9, demonstrating that the three-phase grid current is symmetrical and devoid of dc current.

Case II: Building upon Case I, a dc current of 5 A is introduced into the power grid through the system's feedback path, as illustrated in Fig.10. This clearly indicates the asymmetry of the three-phase grid current.

Case III: In comparison with Case II, the detection outcomes of dc current are assessed and shown in Fig.11, encompassing three detection methodologies (SWDIM-P, SWDIM, and SWSIM methods). Notably, the detection curve (red) of the SWDIM-P aligns with the detection curve (blue) of the conventional integration approach, with a response time of approximately 20 ms. Conversely, the detection curve (green) based on the scheme proposed in [11] exhibits a response time of about two cycles, stabilizing the detection value at 5 A. This confirms the analysis conducted in Case II. Fig.12 shows the dc current detection results with SWDIM-P method, indicating that the dc current can be quickly and accurately detected from the three-phase grid current.

Case IV: Applying the dc current suppression strategy employing the Fuzzy-FOPID controller in Case II, the transient waveform is depicted in Fig.13. Upon injection of dc current, the three-phase grid currents exhibit notable imbalance, subsequently reaching a new equilibrium point after one cycle. This showcases the rapid response capability of the method.

Case V: To validate the effectiveness of the proposed scheme, a comparison is made between Fuzzy-FOPID and the virtual capacitor and BP-PID methods under identical scenarios. Fig.14 illustrates the dc current under the three methodologies. The findings indicate that the proposed Fuzzy-FOPID achieves rapid dc current suppression with minimal overshoot, thereby verifying the validity of the proposed scheme. Fig.15 shows the steady-state of the three-phase grid current with the proposed Fuzzy-FOPID method, indicating that the dc current can be completed eliminated.

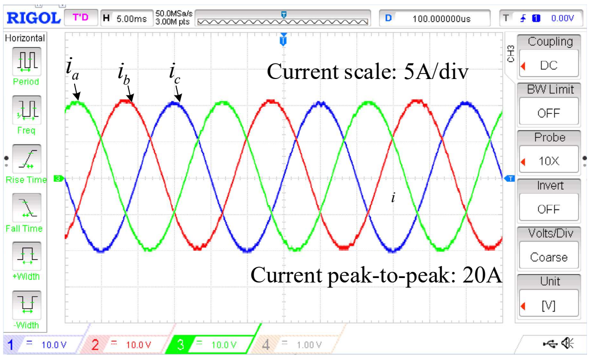

Fig. 9. Steady-state waveform of the three-phase grid current with traditional MPC controller.

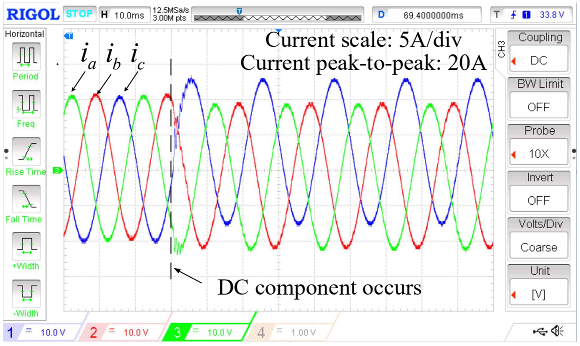

Fig. 10. Transient waveform of the grid current with 5 A dc current.

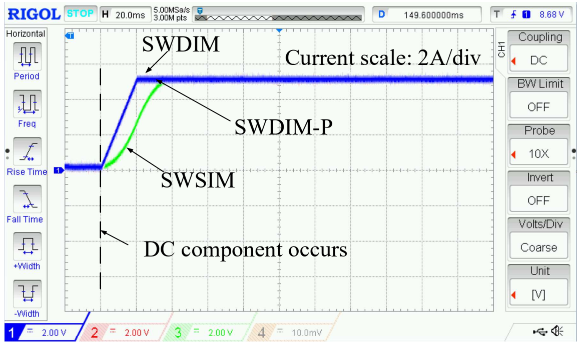

Fig. 11. Comparison of different dc current detection methods.

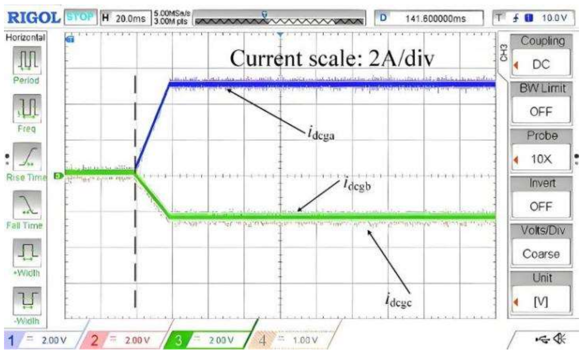

Fig. 12. dc current detection results for the grid current with SWDIM-P.

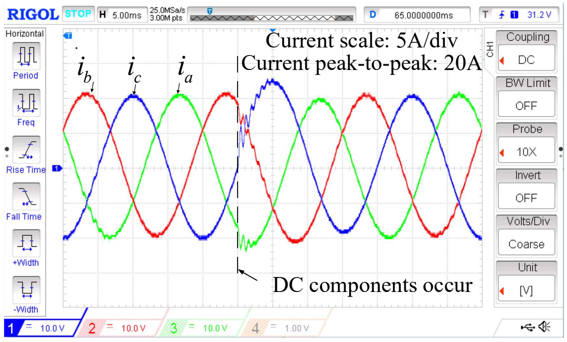

Fig. 13. dc current suppression performance by Fuzzy-FOPID controller.

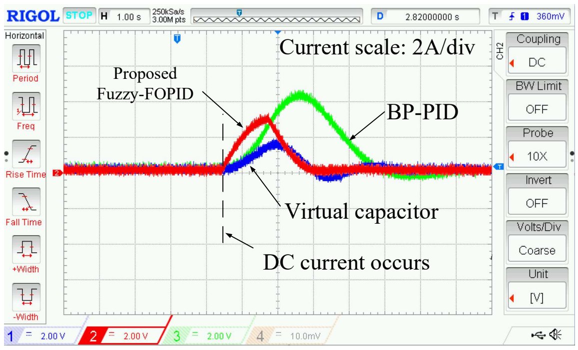

Fig. 14. Comparison of dc current suppression results with different methods.

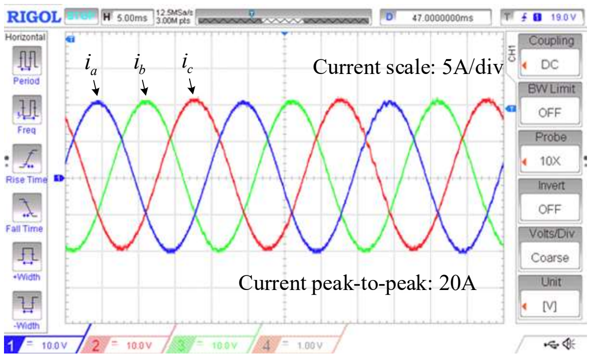

Fig. 15. Steady-state waveform of the three-phase grid current with the proposed Fuzzy-FOPID controller.

VI. Conclusion

In order to attain high-precision, rapid-response, and robust DC current suppression in a non-isolated grid-connected converter, a Fuzzy-FOPID controller based on SWDIM-P is presented. The prediction model of the LCL-GCC is utilized for grid current prediction. Subsequently, the DC current is extracted using the SWIDM method based on the predicted grid current. To achieve multi-objective optimization of control targets (such as grid current, converter-side current, and capacitor voltage), an MPC controller is employed. Both simulation and experimental results indicate that the proposed DC current suppression scheme surpasses traditional schemes (such as BP-PID and virtual capacitor schemes). Future research on DC current suppression could concentrate on multi-level converters for AC motor drive systems.

Reference

[1] Z. Yao, Y. Zhang, and X. Hu, "Transformerless Grid-Connected PV Inverter Without Common Mode Leakage Current and Shoot-Through Problems," *IEEE Transactions on Circuits and Systems II: Express Briefs,* vol. 67, no. 12, pp. 3257-3261, 2020.

[2] E. Giraldo, "Real-time Modified PID Controller over a DC-DC Boost Converter," *IAENG International Journal of Applied Mathematics,* vol. 51, no. 4, pp. 892-898, 2021.

[3] Y. Wei, X. Guo, Z. Zhang, L. Wang, and J. M. Guerrero, "A High-Voltage Gain Transformerless Grid-Connected Inverter," *IEEE Transactions on Industry Applications,* vol. 60, no. 3, pp. 4054-4061, 2024.

[4] A. Srivastava and J. Seshadrinath, "A Novel Single Phase Three Level Triple Boost CG Switched-Capacitor Based Grid-Connected Transformerless PV Inverter," *IEEE Transactions on Industry Applications,* vol. 59, no. 2, pp. 2491-2501, 2023.

[5] S. Pourfarrokh, J. Adabi, and F. Zare, "A New Grid-Connected Asymmetrical Multilevel Converter for PV Application," *IEEE Transactions on Power Electronics,* vol. 39, no. 9, pp. 11256-11265, 2024.

[6] Z. Hu, X. Xing, H. Zhang, and F. Blaabjerg, "Modeling and Suppression Method of Low Order Harmonics for Three-Level Inverter With Small Capacitance Value," *IEEE Transactions on Industrial Electronics,* vol. 72, no. 1, pp. 470-480, 2025.

[7] *IEEE Recommended for practice utility interface of photovoltaic (PV) systems, IEEE 929-2000*, 2000.

[8] M. Chen, D. Xu, T. Zhang, K. Shi, G. He, and K. Rajashekara, "A Novel DC Current Injection Suppression Method for Three-Phase Grid-Connected Inverter Without the Isolation Transformer," *IEEE Transactions on Industrial Electronics,* vol. 65, no. 11, pp. 8656-8666, 2018.

[9] S. N. Vukosavić and L. S. Perić, "High-Precision Sensing of DC Bias in AC Grids," *IEEE Transactions on Power Delivery,* vol. 30, no. 3, pp. 1179-1186, 2015.

[10] "IEEE Standard for Interconnection and Interoperability of Distributed Energy Resources with Associated Electric Power Systems Interfaces--Amendment 1: To Provide More Flexibility for Adoption of Abnormal Operating Performance Category III," *IEEE Std 1547a-2020 (Amendment to IEEE Std 1547-2018),* pp. 1-16, 2020.

[11] W. M. Blewitt, D. J. Atkinson, J. Kelly, and R. A. Lakin, "Approach to low-cost prevention of DC injection in transformerless grid connected inverters," *IET Power Electronics,* vol. 3, no. 1, pp. 111-119, 2010.

[12] G. Qiu, J. Liao, B. Wu, and Z. Shi, "Suppressing DC Current Injection in Transformerless Grid-Connected Inverter Using a Customized Current Sensor," *IEEE Transactions on Power Electronics,* vol. 36, no. 10, pp. 11003-11008, 2021.

[13] W. Zhang, M. Armstrong, and M. A. Elgendy, "DC Injection Suppression in Transformer-less Grid Connected Inverter using a DC Link Current Sensing and Active Control Approach," *IEEE Transactions on Energy Conversion,* vol. 34, no. 1, pp. 396-404, 2018.

[14] L. Zhao, F. Li, Z. Zhuang, Z. Li, and Z. Luo, "A Dual Half-Bridge Converter With Current Doubler Rectifier," *IEEE Transactions on Industrial Electronics,* vol. 67, no. 8, pp. 6398-6406, 2020.

[15] S. Mei *et al.*, "Modified modulation scheme for three-level diode-clamped matrix converter under unbalanced input conditions," *IET Power Electronics,* vol. 11, no. 8, pp. 1425-1433, 2018.

[16] G. Buticchi, E. Lorenzani, and G. Franceschini, "A DC Offset Current Compensation Strategy in Transformerless Grid-Connected Power Converters," *IEEE Transactions on Power Delivery,* vol. 26, no. 4, pp. 2743-2751, 2011.

[17] L. Bowtell and A. Ahfock, " Direct current offset controller for transformerless single-phase photovoltaic grid-connected inverters," vol. 4, no. 5, pp. 432- 437, 2010.

[18] B. Long, L. Huang, H. Sun, Y. Chen, F. Victor, and K. T. Chong, "An intelligent dc current minimization method for transformerless grid-connected photovoltaic inverters," ISA Transactions, vol. 88, pp. 268-279, 2019.

[19] L. Z. Shijie Wang, Peng Wang, Jie Li, Wenqiang Jiang, and Bao Liu, "Feed Forward Cascade PID Based Predictive Control of the PH Value of Desulfurization Slurry in Thermal Power Units," *IAENG International Journal of Computer Science,* vol. 51, no. 7, pp. 842-851, 2024.

[20] A. Abdelhakim, P. Mattavelli, D. S. Yang, and F. Blaabjerg, "Coupled-Inductor-Based DC Current Measurement Technique for Transformerless Grid-Tied Inverters,", *IEEE Transactions on Power Electronics,* vol. 33, no. 1, pp. 18-23, Jan 2018.

[21] D. D. Xiaogao Yang, and Youxin Luo, "Fractional-order Quadratic Time-varying Parameters Discrete Grey Model FQDGM (1, 1) and Its Application," *IAENG International Journal of Applied Mathematics,* vol. 51, no. 4, pp. 1003-1008, 2021.

[22] B. Long, Wei Wang, Lijun Huang, "Design and implementation of a virtual capacitor based DC current suppression method for grid-connected inverters," *ISA Transactions,vol. 92, pp. 257-272,* 2019.

[23] M. Gheisarnejad, H. Farsizadeh, M. R. Tavana, and M. H. Khooban, "A Novel Deep Learning Controller for DC–DC Buck–Boost Converters in Wireless Power Transfer Feeding CPLs," *IEEE Transactions on Industrial Electronics,* vol. 68, no. 7, pp. 6379-6384, 2021.

[24] M. Dashtdar, M. S. Nazir, S. M. S. Hosseinimoghadam, M. Bajaj, and S. Goud B, "Improving the Sharing of Active and Reactive Power of the

Islanded Microgrid Based on Load Voltage Control," *Smart Science,* vol. 10, no. 2, pp. 142-157, 2022/04/03 2022.

[25] W. Wang, P. Wang, T. Bei, and M. Cai, "DC Injection Control for Grid-Connected Single-Phase Inverters Based onn Virtual Capacitor," *Journal of Power Electronics,* vol. 15, no. 5, pp. 1338-1347, 2015.

[26] K. Shinoda, A. Benchaib, J. Dai, and X. Guillaud, "Virtual Capacitor Control: Mitigation of DC Voltage Fluctuations in MMC-based HVDC Systems," *IEEE Transactions on Power Delivery,* pp. 1-1, 2017.

[27] Q. Yan, X. Wu, X. Yuan, Y. Geng, and Q. Zhang, "Minimization of the DC Component in Transformerless Three-Phase Grid-Connected Photovoltaic Inverters," *IEEE Transactions on Power Electronics,* vol. 30, no. 7, pp. 3984-3997, 2015.

[28] J. Scoltock, T. Geyer, and U. K. Madawala, "Model Predictive Direct Power Control for Grid-Connected NPC Converters," *IEEE Transactions on Industrial Electronics,* vol. 62, no. 9, pp. 5319-5328, 2015.

[29] Z. Y. Xiaomin Tian, and Zhen Yang, "Adaptive Stabilization of Fractional-order Energy Supply-demand System with Dead-zone Nonlinear Inputs," *IAENG International Journal of Applied Mathematics,* vol. 49, no. 4, pp. 500-504, 2019.